



November 2007

A Study of Cerium–Manganese Mixed Oxides for Oxidation Catalysis

Gong Zhou
University of Pennsylvania

Parag R. Shah
University of Pennsylvania

Raymond J. Gorte
University of Pennsylvania, gorte@seas.upenn.edu

Follow this and additional works at: http://repository.upenn.edu/cbe_papers

Recommended Citation

Zhou, G., Shah, P. R., & Gorte, R. J. (2007). A Study of Cerium–Manganese Mixed Oxides for Oxidation Catalysis. Retrieved from http://repository.upenn.edu/cbe_papers/104

Postprint version. Published in *Catalysis Letters*, Volume 120, Issue 3-4, January 2008, pages 191-197.
Publisher URL: <http://dx.doi.org/10.1007/s10562-007-9299-y>

This paper is posted at ScholarlyCommons. http://repository.upenn.edu/cbe_papers/104
For more information, please contact libraryrepository@pobox.upenn.edu.

A Study of Cerium–Manganese Mixed Oxides for Oxidation Catalysis

Abstract

Cerium–manganese mixed oxides with compositions of $\text{Ce}_{0.5}\text{Mn}_{0.5}\text{O}_{1.75}$ and $\text{Ce}_{0.8}\text{Mn}_{0.2}\text{O}_{1.9}$ were prepared by the citric-acid (Pechini) method and their catalytic properties were compared to CeO_2 and Mn_2O_3 . The mixed oxides exhibited higher specific rates than either CeO_2 or Mn_2O_3 for oxidation of both methane and n-butane. While XRD measurements of the mixed oxides suggested that the materials had primarily the fluorite structure, oxygen isotherms, measured by coulometric titration at 973 K, exhibited steps associated with MnO – Mn_3O_4 and Mn_3O_4 – Mn_2O_3 equilibria, implying that manganese oxide must exist as separate phases in the solids. The $P(\text{O}_2)$ for the MnO – Mn_3O_4 equilibrium is shifted to lower values in the mixed oxides, indicating that the manganese-oxide phase is affected by interactions with ceria.

Keywords

manganese–cerium mixed oxides, coulometric titration, oxidation–reduction properties, methane oxidation, butane oxidation

Comments

Postprint version. Published in *Catalysis Letters*, Volume 120, Issue 3-4, January 2008, pages 191-197.
Publisher URL: <http://dx.doi.org/10.1007/s10562-007-9299-y>

A Study of Cerium-Manganese Mixed Oxides For Oxidation Catalysis

Gong Zhou, Parag R. Shah, and Raymond J. Gorte
Department of Chemical and Biomolecular Engineering
University of Pennsylvania
Philadelphia, PA 19104, USA

Abstract

Cerium-manganese mixed oxides with compositions of $\text{Ce}_{0.5}\text{Mn}_{0.5}\text{O}_{1.75}$ and $\text{Ce}_{0.8}\text{Mn}_{0.2}\text{O}_{1.9}$ were prepared by the citric-acid (Pechini) method and their catalytic properties were compared to CeO_2 and Mn_2O_3 . The mixed oxides exhibited higher specific rates than either CeO_2 or Mn_2O_3 for oxidation of both methane and n-butane. While XRD measurements of the mixed oxides suggested that the materials had primarily the fluorite structure, oxygen isotherms, measured by coulometric titration at 973 K, exhibited steps associated with $\text{MnO-Mn}_3\text{O}_4$ and $\text{Mn}_3\text{O}_4\text{-Mn}_2\text{O}_3$ equilibria, implying that manganese oxide must exist as separate phases in the solids. The $P(\text{O}_2)$ for the $\text{MnO-Mn}_3\text{O}_4$ equilibrium is shifted to lower values in the mixed oxides, indicating that the manganese-oxide phase is affected by interactions with ceria.

Key Words: Manganese-Cerium mixed oxides, Coulometric titration, oxidation-reduction properties, methane oxidation, butane oxidation.

1. Introduction

Mixed oxides of cerium and manganese ($\text{Ce}_x\text{Mn}_y\text{O}_z$) have received significant attention for a number of catalytic applications, especially in pollution control. For example, $\text{Ce}_x\text{Mn}_y\text{O}_z$ is known to be active for catalytic wet oxidation, where water is the oxidant, to remove hydrocarbon pollutants from aqueous streams [1-8]. More recently, the mixed oxides have been shown to have a significantly lower light-off temperature for oxidation of diesel soot compared to the individual oxides [9] and to be selective for catalytic reduction of NO_x with ammonia [10-14]. In both of these applications, the mixed oxides show properties superior to the individual oxides, in part because of the ability of $\text{Ce}_x\text{Mn}_y\text{O}_z$ to oxidize NO to NO_2 and to then store adsorbed NO_2 on its surface. Most recently, the mixed oxides have been suggested to have potential for H_2 production by two-step splitting of water [15]. In this example, $\text{Ce}_x\text{Mn}_y\text{O}_z$ is reduced by heating to high temperatures and then re-oxidized by steam to produce H_2 .

Enhanced reducibility of the mixed oxides is key in each of these applications and has indeed been inferred from temperature-programmed reduction (TPR) measurements [6,16-19]. However, while TPR measurements can be used to quantify the reduction extent of a material, the characteristic temperature at which reduction occurs is only a qualitative measure of the ease with which a material reduces [20]. This is especially true for materials that undergo bulk reduction, since diffusion of oxygen to the surface must precede reaction. A more quantitative measure of reducibility involves determining thermodynamic properties, such as enthalpy or free-energy changes associated with oxidation and reduction of a material. That ceria-based mixed oxides can exhibit enhanced reducibility is clear from the example of ceria-zirconia oxides ($\text{Ce}_x\text{Zr}_{(1-x)}\text{O}_2$), which find wide-scale application for oxygen-storage capacitance (OSC) [21-27]. The high reducibility of $\text{Ce}_x\text{Zr}_{(1-x)}\text{O}_2$ is easily explained by the small enthalpy change associated with reduction [28-30]. Compared to reduction of CeO_2 , the magnitude of the enthalpy change associated with reduction of $\text{Ce}_x\text{Zr}_{(1-x)}\text{O}_2$ is lower by approximately 250 kJ/mol O_2 .

In the case of $\text{Ce}_x\text{Zr}_{(1-x)}\text{O}_2$, enhanced reducibility is at least partially due to formation of solid solutions [28-30]. The individual oxides and the mixed oxides exist in a fluorite structure, and the lattice parameters of ceria-zirconia mixed oxides vary linearly with composition. With $\text{Ce}_x\text{Mn}_y\text{O}_z$, the structure of the most active phases is less clear and the catalytic properties depend strongly on how the material is prepared. For example, Wu, et al [31] examined

$\text{Ce}_{0.5}\text{Mn}_{0.5}\text{O}_2$ prepared by citric-acid, sol-gel method and reported that the XRD results showed a very small lattice parameter shift and finely dispersed Mn_3O_4 peaks in the diffraction pattern. They concluded that the high reducibility and catalytic activity of the mixed oxides were associated with strong interactions between Mn and Ce. Kaneko, et al [15] argued for the formation of $\text{Ce}_{0.9}\text{Mn}_{0.1}\text{O}_2$ solid solutions but observed no shift in the lattice parameter compared to pure ceria. Qi and Yang [11] reported evidence for three different phases in $\text{Mn}_{0.3}\text{Ce}_{0.7}\text{O}_x$ prepared by the citric-acid method: (1) aggregated Mn_2O_3 on the CeO_2 support, (2) highly dispersed Mn_2O_3 with strong interactions with CeO_2 , and (3) Mn atoms incorporated into the CeO_2 lattice with very little lattice parameter shift. While Murugan, et al [19] reported that the structure of $\text{Ce}_x\text{Mn}_y\text{O}_z$ depends strongly on the preparation procedure, they reported that there is a small shift in the fluorite lattice parameter upon addition of Mn.

In the present study, we investigated the redox properties of $\text{Ce}_{0.8}\text{Mn}_{0.2}\text{O}_{1.9}$ and $\text{Ce}_{0.5}\text{Mn}_{0.5}\text{O}_{1.75}$ by measuring the oxidation isotherms at 973 K. The materials were prepared by the citric-acid (Pechini) method, since this leads to materials with the best mixing of the oxides. Because the equilibrium constant for oxidation of a solid to another solid is proportional to the equilibrium oxygen fugacity, $P(\text{O}_2)$, the oxidation isotherms can be used to calculate the Gibbs Free Energy change, ΔG , for oxidation for any solid (e.g. $\text{Ce}_x\text{Mn}_y\text{O}_z$) as a function of the oxygen stoichiometry. The range of $P(\text{O}_2)$ values that are of interest for equilibrium measurements with most catalytic oxides is so low as to be experimentally inaccessible; however, low $P(\text{O}_2)$ can be established through equilibrium with H_2 oxidation, $\text{H}_2 + \frac{1}{2}\text{O}_2 = \text{H}_2\text{O}$, as discussed in detail elsewhere [28-30,32]. Although the $\text{Ce}_{0.8}\text{Mn}_{0.2}\text{O}_{1.9}$ and $\text{Ce}_{0.5}\text{Mn}_{0.5}\text{O}_{1.75}$ samples exhibited higher specific rates for oxidation of both methane and butane than either of the pure oxides, the oxygen isotherms for the mixed oxides are similar to what would be expect for a physical mixture of CeO_2 and Mn_2O_3 , suggesting that these are not solid solutions.

2. Experimental Section

2.1 Samples

The pure ceria and manganese oxides were prepared in our laboratory by decomposition of $\text{Ce}(\text{NO}_3)_3 \cdot 4\text{H}_2\text{O}$ (99.5%, Alfa Aesar) and $\text{Mn}(\text{NO}_3)_2 \cdot 4\text{H}_2\text{O}$ (99.98%, Alfa Aesar) at 723K and 973 K, respectively. The $\text{Ce}_{0.8}\text{Mn}_{0.2}\text{O}_{1.9}$ and $\text{Ce}_{0.5}\text{Mn}_{0.5}\text{O}_{1.75}$ samples were prepared using the citric-acid method, since this method is expected to optimize mixing of the metal cations in the solid and since materials prepared in this way appear to have the best catalytic properties [12].

Stoichiometric amounts of $\text{Ce}(\text{NO}_3)_3$ and $\text{Mn}(\text{NO}_3)_2$ were dissolved in distilled water and then mixed with aqueous citric acid ($\geq 99.5\%$, Aldrich) to produce a solution with a citric-acid:metal-ion ratio of 2:1. After vigorous stirring for 1 h at room temperature, the water was removed by evaporation with mild heating. The resulting solids were calcined in air at 973 K for 5 hours to produce the mixed oxide solutions. Finally, the samples were characterized by x-ray diffraction (XRD), using a Rigaku Geigerflex diffractometer with $\text{CuK}\alpha$ radiation ($\lambda = 1.5405 \text{ \AA}$), and by BET measurements. The lattice parameters for selected samples having the fluorite structure were also determined from the location of the (220) diffraction peak, using NaCl as an internal reference.

2.2 Catalytic Studies

Both methane-oxidation and butane-oxidation rates were used to characterize the catalytic properties of the materials. Rate measurements were performed in a $\frac{1}{4}$ -inch, Pyrex, tubular reactor using approximately 0.10 g of catalyst. The total feed rate to the reactor was maintained at 120 ml/min, and the partial pressures of CH_4 , C_4H_{10} , O_2 , and He were controlled by adjusting the relative flow rates of each component. Methane-oxidation rates were obtained in 50 torr of CH_4 and 100 torr of O_2 for methane-oxidation. Butane-oxidation rates were obtained in 12.6 torr n-butane and 100 torr O_2 . For all measurements where rates are reported, the conversions of CH_4 and O_2 were kept well below 10%, so that differential conditions could be assumed. All reaction rates are normalized to the BET surface areas of the samples. The concentration of the effluent from the reactor was determined using an on-line, gas chromatograph, SRI8610C, equipped with a Haysep Q column and a TCD detector.

2.3 Equilibrium Measurements

The equilibrium isotherms were measured using coulometric titration in an apparatus that has been described in previous publications [28,29,32]. In coulometric titration, the $P(\text{O}_2)$ of the gases over an equilibrated sample are measured electrochemically with an oxygen sensor. For this study, the samples were placed in a sealed container at 973 K and reduced in a flowing mixture of 90% He and 10% H_2 for approximately 1 h. After having been reduced, the samples were sealed in the gas mixture and the equilibrium $P(\text{O}_2)$ were measured using an oxygen sensor that is essentially a solid oxide fuel cell with a yttria-stabilized zirconia (YSZ) membrane. The electrodes for the sensor were made from Ag paste on the reducing side and a composite of YSZ and $\text{La}_{0.8}\text{Sr}_{0.2}\text{MnO}_3$ (LSM) on the air side. In addition to measuring the $P(\text{O}_2)$, the sensor was

also used to add oxygen to the samples through application of a potential across the ion-conducting, YSZ membrane. A precise amount of charge could be passed across the membrane using a Gamry Instruments potentiometer, with 1 Coulomb of charge equivalent to 2.6 $\mu\text{mol O}_2$.

To address the question of whether high-temperature reduction could remove Mn ions from ceria lattice, we modified the electrode of one cell to allow measurement of the isotherm starting from an oxidized sample. To allow pumping of oxygen from the cell, a thin layer of ceria-zirconia (~ 1 mg of ceria) was added between the Ag paste and the YSZ wafer. The fresh sample was then exposed to a flowing mixture of 10% H_2O , 5% O_2 , and 85% Ar for approximately 0.5 h at 973 K and then sealed in the gas mixture. With this cell, it was possible to measure the isotherm from both oxidizing and reducing conditions.

Since 10^{-20} atm corresponds to less than one molecule in the entire coulometric-titration apparatus, it is important to recognize that the measured $P(\text{O}_2)$ are fugacities established by equilibrium between H_2 and H_2O over most of the $P(\text{O}_2)$ range that was investigated. The criterion we used for establishing equilibrium in coulometric titration was that the potential of the oxygen sensor change by less than 1 mV/h. The time required for achieving equilibrium was typically one or two days after the addition of oxygen to the sample.

3. Results

3.1 XRD Characterization

Fig. 1 shows the XRD patterns for the CeO_2 , $\text{Ce}_{0.8}\text{Mn}_{0.2}\text{O}_{1.9}$, and $\text{Ce}_{0.5}\text{Mn}_{0.5}\text{O}_{1.75}$ samples immediately after calcination at 973 K. In each case, the main peaks in the patterns are those of a fluorite structure similar to that of pure ceria, although a small shoulder at 36 degrees 2θ in the pattern for the $\text{Ce}_{0.5}\text{Mn}_{0.5}\text{O}_{1.75}$ sample in Fig. 1a) is indicative of Mn_3O_4 . No peaks associated with an Mn_2O_3 phase were observed. However, the diffraction lines were very broad, and the highest intensity peaks for Mn_2O_3 are located at 33 and 55.2 degrees 2θ where the fluorite structure of CeO_2 also shows high intensity peaks (The (200) peak at 33 degrees 2θ and the (311) peak at 56.3 degrees 2θ are primarily associated with the fluorite structure.). The formation of solid solutions obviously cannot be inferred from the absence of peaks.

Because reduction causes changes in the samples, XRD patterns are shown in Fig. 2 for the two mixed oxides after reduction at 973 K in 90% N_2 and 10% H_2 for 1 h, followed by oxidation in 2% O_2 at 973 K. The low re-oxidation pressure for O_2 was chosen because oxidation of MnO under these conditions gave Mn_3O_4 , which is easier to observe in XRD patterns of the

mixed oxides. The patterns for the $\text{Ce}_{0.8}\text{Mn}_{0.2}\text{O}_{1.9}$ and $\text{Ce}_{0.5}\text{Mn}_{0.5}\text{O}_{1.75}$ samples were significantly affected. First, there was a narrowing of the peaks associated with the fluorite phase, implying a growth in the crystallite size. Both Mn-containing samples also exhibit multiple peaks associated with an Mn_3O_4 phase, for which the largest peak (the (211) peak) is located at 36.3 degrees 2θ . Again, no peaks assignable to the Mn_2O_3 phase were observed. For $\text{Ce}_{0.8}\text{Mn}_{0.2}\text{O}_{1.9}$, we attempted to form the Mn_2O_3 phase by oxidizing the sample in pure O_2 at 973 K but no changes were observed following this treatment.

Because shifts in the lattice parameter with composition are usually more definitive in demonstrating the formation of solid solutions, we measured the lattice parameter of the $\text{Ce}_{0.8}\text{Mn}_{0.2}\text{O}_{1.9}$ sample after reduction and oxidation at 973 K. The lattice parameter of the fluorite phase was calculated to be 0.54066 nm based on the location of the (220) diffraction peak. Although a previous study of a material with the same composition and essentially the same lattice parameter, 0.54059 nm, argued the mixed oxide was a solid solution [19], this lattice parameter is too close to that of pure ceria (0.5414 nm) to make the assignment firm.

3.2 Hydrocarbon Oxidation Rates

To determine how the activity depends on the manganese concentration, we compared the methane and butane oxidation rates over Ceria, Mn_2O_3 , $\text{Ce}_{0.8}\text{Mn}_{0.2}\text{O}_{1.9}$, and $\text{Ce}_{0.5}\text{Mn}_{0.5}\text{O}_{1.75}$. Arrhenius plots for methane oxidation are shown in Fig. 3a), with activation energies reported in Table 1. The methane-oxidation rates were similar on the two mixed oxides and higher than that observed on either Mn_2O_3 or CeO_2 . The activation energies on the Mn-containing samples were also significantly lower than on CeO_2 . The reaction rates for butane oxidation on Ceria, Mn_2O_3 , and $\text{Ce}_{0.8}\text{Mn}_{0.2}\text{O}_{1.9}$ are reported in Fig. 3b). Again, the ceria-manganese mixed oxide sample exhibited higher reaction rates than either CeO_2 or Mn_2O_3 .

3.3 Thermodynamic measurements

Fig. 4 shows the O_2 isotherms for ceria and manganese oxide at 973 K, measured using coulometric titration. After equilibration, following sample reduction in a flowing mixture of 90% N_2 and 10% H_2 for 1 h at 973 K, the O_2 fugacity was between 10^{-26} and 10^{-24} atm for both samples. In this range of $P(\text{O}_2)$, ceria should be only slightly reduced. Based on previous thermodynamic measurements [28,30], the equilibrium, O:Ce ratio at 10^{-24} atm is greater than 1.97. In agreement with this, very little oxygen was taken up by the ceria sample when the oxygen fugacity was raised to above 10^{-2} atm.

By contrast, manganese oxide is expected to exist as MnO at a $P(O_2)$ of 10^{-24} atm and is expected to take up 6.3 mmol O/g Mn_2O_3 in order to form Mn_2O_3 . In agreement with this, the isotherm for MnO_x exhibits two steps at $P(O_2)$ near 10^{-10} atm and 10^{-2} atm, with a total uptake of oxygen close to that predicted from the stoichiometries of MnO and Mn_2O_3 . The first step occurs with the addition of 4.2 mmol O/g Mn_2O_3 and is associated with the formation of Mn_3O_4 . The second step occurs with the addition an extra 2.1 mmol O/g Mn_2O_3 and involves formation of Mn_2O_3 . The $P(O_2)$ values at these steps agree well with the literature values for the thermodynamic equilibria, which indicate an equilibrium $P(O_2)$ of 1.5×10^{-11} atm for the reaction $6 MnO + O_2 = 2 Mn_3O_4$ and 7×10^{-2} atm for the reaction $4 Mn_3O_4 + O_2 = 6 Mn_2O_3$ at 973 K [33], especially considering that the literature equilibrium data had to be extrapolated from lower temperatures.

The oxygen isotherms at 973 K are shown for the $Ce_{0.5}Mn_{0.5}O_{1.75}$, $Ce_{0.8}Mn_{0.2}O_{1.9}$, and Mn_2O_3 samples in Figure 5. In order to emphasize the similarities between the samples, we have normalized the amount of oxygen that was added to the molar content of Mn in each sample. Also, while the samples were initially reduced to lower $P(O_2)$ by the treatment in 10% H_2 at 973 K, we have chosen to consider only the oxygen added after the $P(O_2)$ rose above 10^{-21} atm. The amount of oxygen required to raise the $P(O_2)$ from its initial value to above 10^{-21} atm on each of the ceria-containing samples was small, essentially identical to that shown for pure CeO_2 in Fig. 3. The amount of oxygen taken up by ceria was only significant compared to the Mn content for the $Ce_{0.8}Mn_{0.2}O_{1.9}$ sample. Due to the relatively small amount of Mn in that particular sample, it is likely that most of the oxygen that was added in taking the $P(O_2)$ from 10^{-21} atm to 10^{-14} atm is associated with the ceria oxidation.

Clearly, the isotherms for the Mn-containing samples in Fig. 5 are similar, each showing steps in a $P(O_2)$ range corresponding to oxidation of MnO to Mn_3O_4 and to oxidation of Mn_3O_4 to Mn_2O_3 . (For the $Ce_{0.5}Mn_{0.5}O_{1.75}$ sample, the isotherm was stopped before completing the transition from Mn_3O_4 to Mn_2O_3 .) The overall consumption of oxygen per Mn in each sample was also very close to the amounts expected for each transition, 0.33 mol-O/mol-Mn for reaction of MnO to Mn_3O_4 and 0.17 mol-O/mol-Mn and for reaction of Mn_3O_4 to Mn_2O_3 . (For the $Ce_{0.8}Mn_{0.2}O_{1.9}$ sample, we have ignored the oxygen associated with taking the oxygen fugacity from 10^{-21} atm to 10^{-13} atm, since oxygen is likely associated with ceria, as discussed above.) The data leads to an important conclusion. Assuming that the first step does indeed correspond to

reaction of MnO to Mn₃O₄, the Mn ions must exist in relatively large domains. If there were isolated Mn ions in a ceria framework, it would seem unlikely that there would be an equilibrium between the reduced and oxidized species that would be similar to the one between MnO and Mn₃O₄, since Mn₃O₄ has Mn ions of mixed valency. The fact that the oxygen stoichiometries match the Mn contents suggests that all of the Mn accounted for. In other words, the concentration of isolated Mn ions must be small. Finally, the data suggest that ceria affects the equilibrium P(O₂) where MnO reacts to Mn₃O₄. The Ce_{0.5}Mn_{0.5}O_{1.75} and Ce_{0.8}Mn_{0.2}O_{1.9} samples are oxidized at somewhat lower P(O₂) than that measured on the manganese oxide sample.

One possible issue with the above measurements is that the Mn ions may have come out of the solution with the ceria during the high-temperature reduction. Therefore, we repeated the isotherm measurements on the Ce_{0.8}Mn_{0.2}O_{1.9} sample, starting from the freshly oxidized sample, with the results shown in Fig. 6. While the scale in Fig. 6 is referenced to the completely reduced sample, the oxygen was removed from the sample starting from its state after oxidation in 10% H₂O, 5% O₂, and 85% Ar. Initially, the P(O₂) decreased almost linearly while oxygen was being removed in a manner similar to that observed for high-surface-area ceria [32]. As we continued removing oxygen from the sample, a transition from Mn₃O₄ to MnO was clearly observed. After the transition, the change in P(O₂) with oxygen removal was again gradual, similar to what is observed with high-surface-area ceria. After reaching a P(O₂) 10⁻²⁰ atm, a second isotherm was measured by adding oxygen to the sample. The second isotherm is almost identical to the first but with less uptake after the transition from MnO to Mn₃O₄. The overall removal/addition of oxygen per Mn in Ce_{0.8}Mn_{0.2}O_{1.9} was approximately 0.3 mol-O/mol-Mn for reaction of MnO to Mn₃O₄, similar to what we had observed in figure 5. **However, the transition between MnO to Mn₃O₄ occurred at slightly higher P(O₂) compared to the one shown in Fig 5.** We suggest that the subtle differences are possibly due to the sintering of Mn in the mixture for the highly reduced sample. Interestingly, we did not see a transition from Mn₃O₄ to Mn₂O₃ of the freshly oxidized sample, in agreement with the XRD results which suggested that the manganese oxide exists as Mn₃O₄ after calcination.

4. Discussion

What we set out to establish in this study was whether mixed oxides of cerium and manganese could form solid solutions and whether interactions between the two oxides enhanced activity for simple hydrocarbon-oxidation reactions. The primary conclusions are that

interactions between ceria and manganese oxide phases lead to enhanced catalytic activity, but that solid solutions are not formed. Regarding the formation of solid solutions, the small size of peaks associated with manganese-oxide phases in the XRD data is clearly not definitive in determining whether or not solid solutions form. The fact that there is no significant shift from that of pure ceria in the lattice parameter for the fluorite structure is a strong indication that Mn ions do not substitute into this lattice. Furthermore, the equilibrium transition between MnO and Mn₃O₄ phases in the isotherms on each of the samples is difficult to understand unless one assumes that there is a separate manganese-oxide phase.

Obviously, the conclusion reached from the data on our samples, that Mn does not substitute for Ce in the fluorite lattice, may not be true for all different ways in which the mixed oxides could be prepared. However, the synthesis method used in this study, the Pechini method, was that which typically leads to the best mixing of the metal ions. While the relatively high-temperatures we used to treat the materials may have caused phase separation, the fact that the phase separation is so complete, even for materials with the relatively dilute composition of Ce_{0.8}Mn_{0.2}O_{1.9}, suggests that the Mn ions never were in the lattice or can be removed very easily.

It is interesting to consider why the mixed oxides showed a higher catalytic activity than either of the individual oxides and it is tempting to suggest that this is related to lower P(O₂) observed in the isotherms for the oxidation of MnO to Mn₃O₄ in the Ce_{0.5}Mn_{0.5}O_{1.75} and Ce_{0.8}Mn_{0.2}O_{1.9} samples. On the Ce_{0.8}Mn_{0.2}O_{1.9} sample, this transition occurs below 10⁻¹³ atm, a value much lower than that which we measured on Mn₂O₃. The implication is that the Mn ions in ceria-containing samples are more easily oxidized, which in turn suggests strong interactions between ceria and manganese oxide as others have also suggested. One possibility is that there is a transfer of oxygen from ceria, which is easily oxidized, to the supported manganese-oxide cluster. Oxygen transfer from ceria has been suggested in many studies of ceria-supported metals. For example, Smirnov and Graham [34] showed that Pd films that had been vapor deposited onto ceria-zirconia substrates could be completely oxidized by heating to 423 K in ultra-high vacuum. Given that oxygen binding is much stronger on reduced ceria-zirconia than it is on Pd [28,30,35], this transfer of oxygen must be endothermic, suggesting that the driving force for oxygen transfer from ceria-zirconia to Pd is entropic. A similar situation may occur with CeO₂ and MnO, even though this reaction should also be endothermic.

The results here for mixed oxides of cerium and manganese demonstrate that mixed oxides can have interesting properties, even if they are not solid solutions. Understanding the reasons behind the interactions between the two phases remains an interesting problem in catalysis.

5. Conclusions

Our results indicate that mixed oxides of cerium and manganese do not form solid solutions. While XRD results on the mixed oxides could be interpreted as resulting from a fluorite structure with Mn ions substituted for some of the Ce ions, oxygen isotherms show that almost all of the manganese oxide is associated with a separate phase. However, interactions between the manganese oxide and the ceria cause the mixed oxide to be more active for hydrocarbon-oxidation reactions than either ceria or manganese oxide individually.

Acknowledgements:

This work was supported by the Department of Energy, Office of Basic Energy Sciences, Chemical Sciences, Geosciences and Biosciences Division, Grant DE-FG02-85ER13350.

References:

- [1] S.K. Bhargava, J. Tardio, J. Prasad, K. Foger, D.B. Akolekar, S.C. Grocott, *Ind. Eng. Chem. Res.* 45 (2006) 1221.
- [2] M. Abecassis-Wolfovich, R. Jothiramalingam, M.V. Landau, M. Herskowitz, B. Viswanathan, T.K. Varadarajan, *Applied Catalysis B: Environmental* 59 (2005) 91.
- [3] A.M.T. Silva, R.R.N. Marques, R.M. Quinta-Ferreira, *Applied Catalysis B: Environmental* 47 (2004) 269.
- [4] S. Imamura, in A. Trovarelli (Editor), *Catalysis by Ceria and Related Materials*, Imperial College Press; London, 2002.
- [5] S.T. Hussain, A. Sayari, F. Larachi, *Applied Catalysis B: Environmental* 34 (2001) 1.
- [6] H. Chen, A. Sayari, A. Adnot, F. Larachi, *Applied Catalysis B: Environmental* 32 (2001) 195.
- [7] Y.I. Matatov-Meytal, M. Sheintuch, *Ind. Eng. Chem. Res.* 37 (1998) 309.
- [8] S. Hamoudi, F. Larachi, A. Sayari, *Journal of Catalysis* 177 (1998) 247.
- [9] K. Tikhomirov, O. Krocher, M. Elsener, A. Wokaun, *Applied Catalysis B: Environmental* 64 (2006) 72.
- [10] F. Eigenmann, M. Maciejewski, A. Baiker, *Applied Catalysis B: Environmental* 62 (2006) 311.
- [11] G. Qi, R.T. Yang, *J. Phys. Chem. B* 108 (2004) 15738.
- [12] G. Qi, R.T. Yang, *Journal of Catalysis* 217 (2003) 434.
- [13] M. Machida, M. Uto, D. Kurogi, T. Kijima, *Chem. Mater.* 12 (2000) 3158.
- [14] M. Machida, D. Kurogi, T. Kijima, *Chem. Mater.* 12 (2000) 3165.
- [15] H. Kaneko, T. Miura, H. Ishihara, S. Taku, T. Yokoyama, H. Nakajima, Y. Tamaura, *Energy* 32 (2007) 656.
- [16] G. Picasso, M. Gutierrez, M.P. Pina, J. Herguido, *Chemical Engineering Journal* 126 (2007) 119.
- [17] F. Arena, G. Trunfio, J. Negro, B. Fazio, L. Spadaro, *Chem. Mater.* 19 (2007) 2269.
- [18] X. Tang, Y. Li, X. Huang, Y. Xu, H. Zhu, J. Wang, W. Shen, *Applied Catalysis B: Environmental* 62 (2006) 265.
- [19] B. Murugan, A.V. Ramaswamy, D. Srinivas, C.S. Gopinath, V. Ramaswamy, *Chem. Mater.* 17 (2005) 3983.
- [20] R.J. Gorte, *Catalysis Today* 28 (1996) 405.
- [21] H. Shinjoh, *Journal of Alloys and Compounds* 408-412 (2006) 1061.
- [22] M. Sugiura, M. Ozawa, A. Suda, T. Suzuki, T. Kanazawa, *Bulletin of the Chemical Society of Japan* 78 (2005) 752.
- [23] J. Kaspar, P. Fornasiero, N. Hickey, *Catalysis Today* 77 (2003) 419.
- [24] M. Shelef, G.W. Graham, R.W. McCabe, in A. Trovarelli (Editor), *Catalysis by Ceria and Related Materials*, Imperial College Press; London, 2002.
- [25] T. Masui, T. Ozaki, K.-i. Machida, G.-y. Adachi, *Journal of Alloys and Compounds* 303-304 (2000) 49.
- [26] R.W. McCabe, J.M. Kisenyi, *Chemistry & Industry* (1995) 605.
- [27] M. Ozawa, M. Kimura, A. Isogai, *Journal of Alloys and Compounds* 193 (1993) 73.
- [28] G. Zhou, P.R. Shah, T. Kim, P. Fornasiero, R.J. Gorte, *Catalysis Today* 123 (2007) 86.
- [29] P.R. Shah, T. Kim, G. Zhou, P. Fornasiero, R.J. Gorte, *Chemistry of Materials* 18 (2006) 5363.

- [30] T. Kim, J.M. Vohs, R.J. Gorte, *Industrial & Engineering Chemistry Research* 45 (2006) 5561.
- [31] X. Wu, Q. Liang, D. Weng, J. Fan, R. Ran, *Catalysis Today* 126 (2007) 430.
- [32] G. Zhou, P.R. Shah, T. Montini, P. Fornasiero, R.J. Gorte, *Surface Science* 601 (2007) 2512.
- [33] S. Fritsch, A. Navrotsky, *Journal of the American Ceramic Society* 79 (1996) 1761.
- [34] M.Y. Smirnov, G.W. Graham, *Catalysis Letters* 72 (2001) 39.
- [35] J.S. Warner, *Journal of The Electrochemical Society* 114 (1967) 68.

Table 1. Surface areas and activation energies (EA) for each of the catalysts.

| Sample | Surface area (m ² /g) | Methane oxidization EA (kJ/mol) | Butane oxidization EA (kJ/mol) |
|--|-------------------------------------|------------------------------------|-----------------------------------|
| CeO ₂ | 94 | 129 | 105 |
| Mn ₂ O ₃ | 34 | 90 | 113 |
| Ce _{0.8} Mn _{0.2} O _y | 35 | 98 | 96 |
| Ce _{0.5} Mn _{0.5} O _y | 78 | 95 | - |

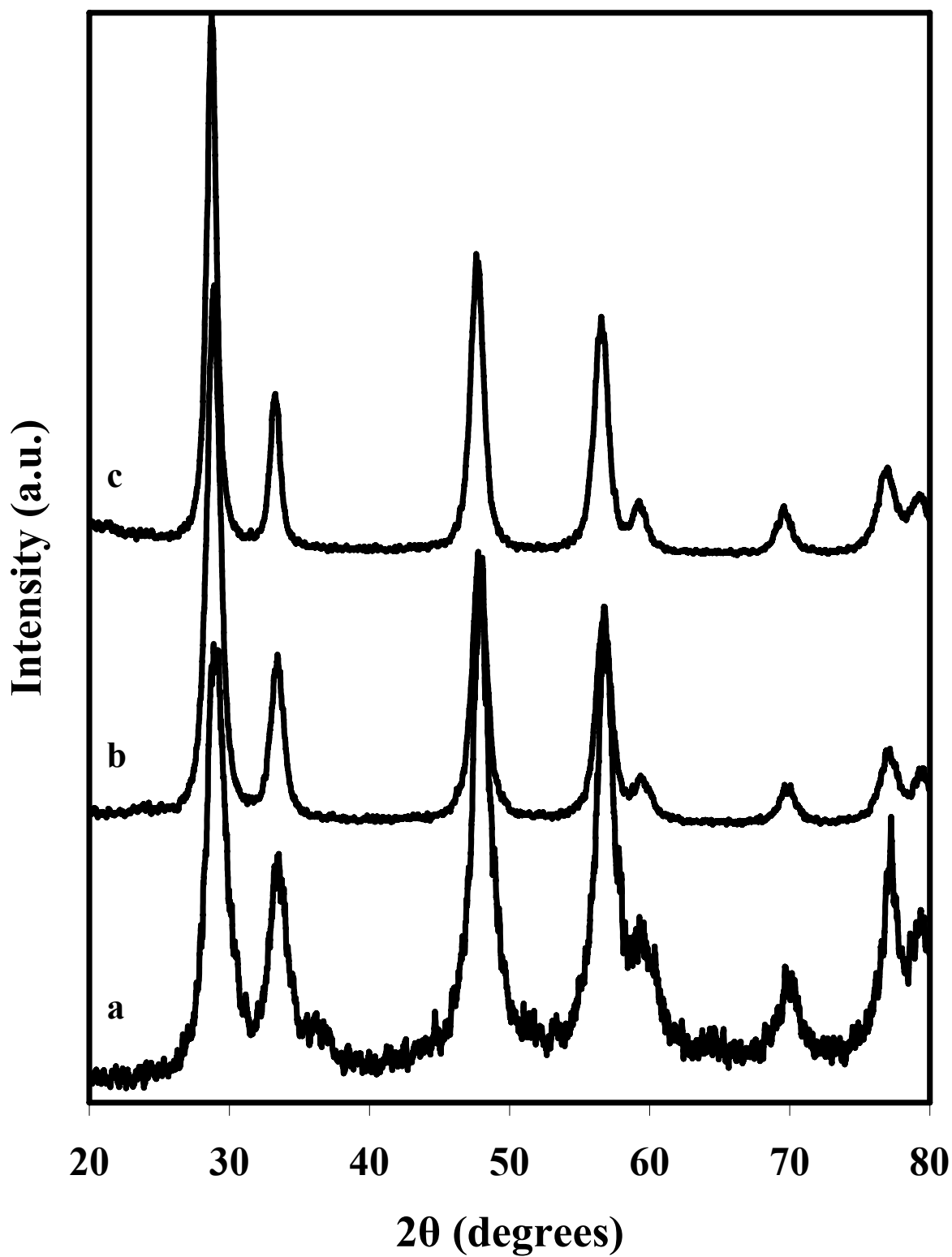


Figure 1. XRD patterns for cerium-manganese mixed oxides prepared using the citric-acid (Pechini) method, followed by calcination in air at 973 K. a) $\text{Ce}_{0.5}\text{Mn}_{0.5}\text{O}_{1.75}$, b) $\text{Ce}_{0.8}\text{Mn}_{0.2}\text{O}_{1.9}$, and c) CeO_2 .

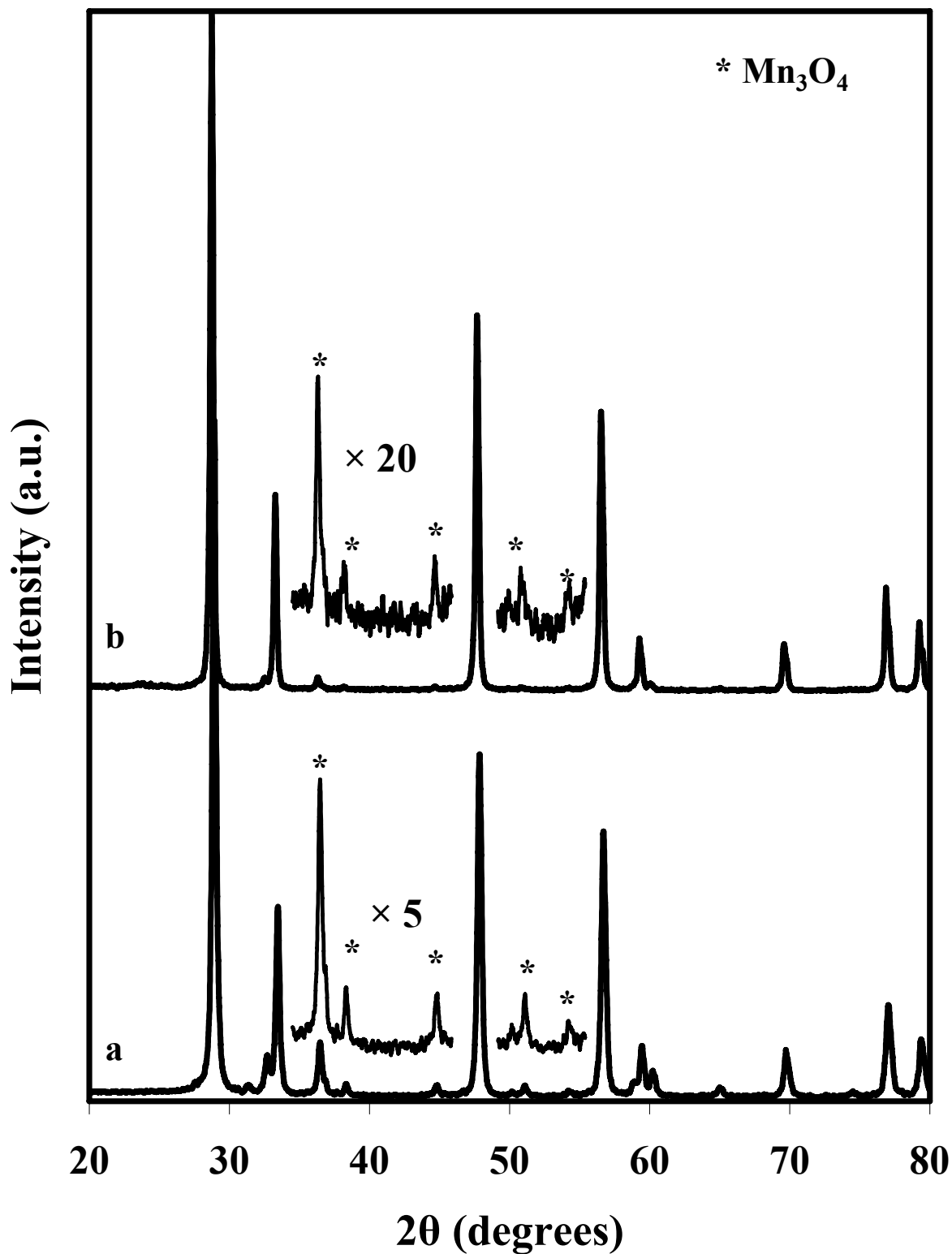


Figure 2. XRD patterns for a) Ce_{0.5}Mn_{0.5}O_{1.75} and b) Ce_{0.8}Mn_{0.2}O_{1.9}, after reduction in 10% H₂ at 973 K, followed by oxidation in 2% O₂. Asterisks show peaks that are associated with Mn₃O₄, the stable phase of manganese oxide under these oxidizing conditions.

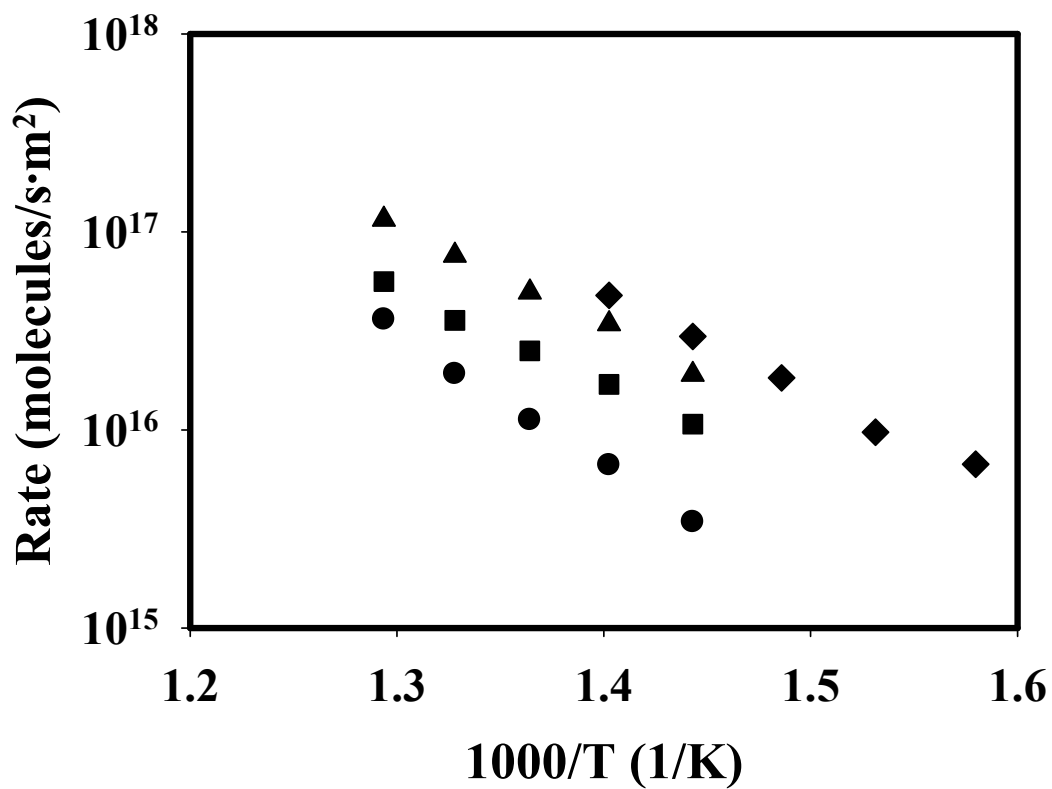


Figure 3a). Differential reaction rates for methane oxidation on the following catalysts: (\bullet) CeO_2 , (\blacksquare) Mn_2O_3 , (\blacktriangle) $\text{Ce}_{0.8}\text{Mn}_{0.2}\text{O}_{1.9}$, and (\blacklozenge) $\text{Ce}_{0.5}\text{Mn}_{0.5}\text{O}_{1.75}$. The reaction was carried out at partial pressures of 50 torr for CH_4 and 100 torr of O_2 .

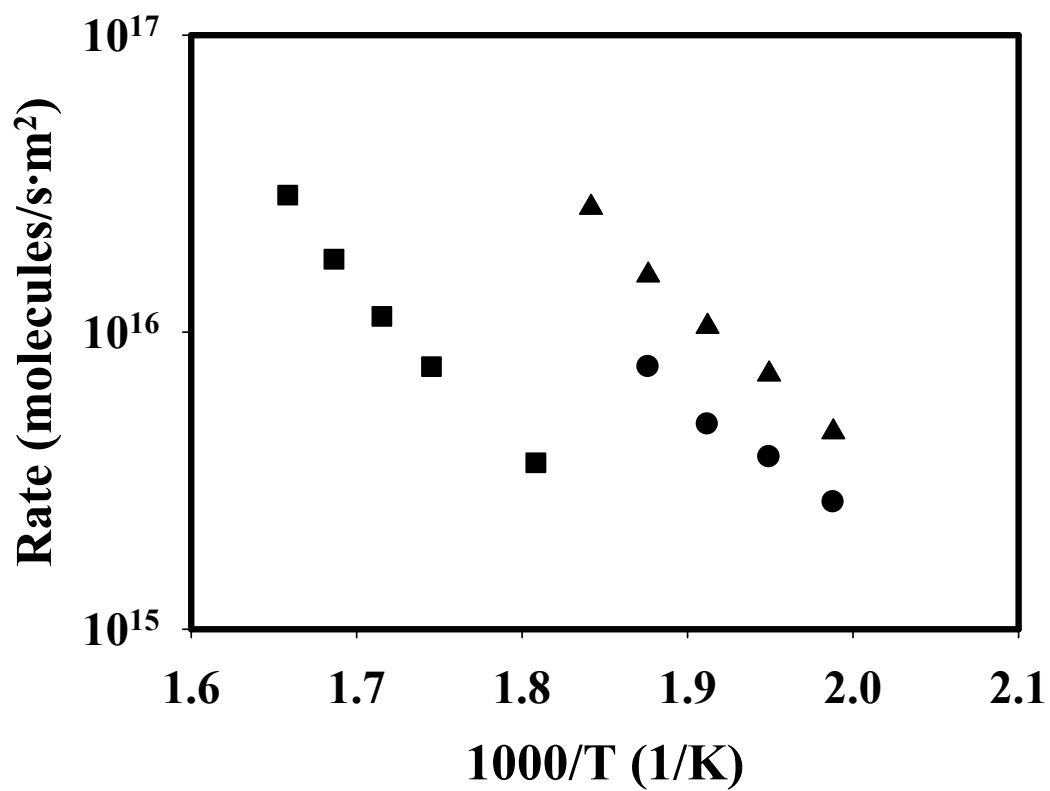


Figure 3b). Differential reaction rates for methane oxidation on the following catalysts: (●) CeO₂, (■) Mn₂O₃, and (▲) Ce_{0.8}Mn_{0.2}O_{1.9}. The reaction was carried out at partial pressures of 12.6 torr for n-butane and 100 torr of O₂.

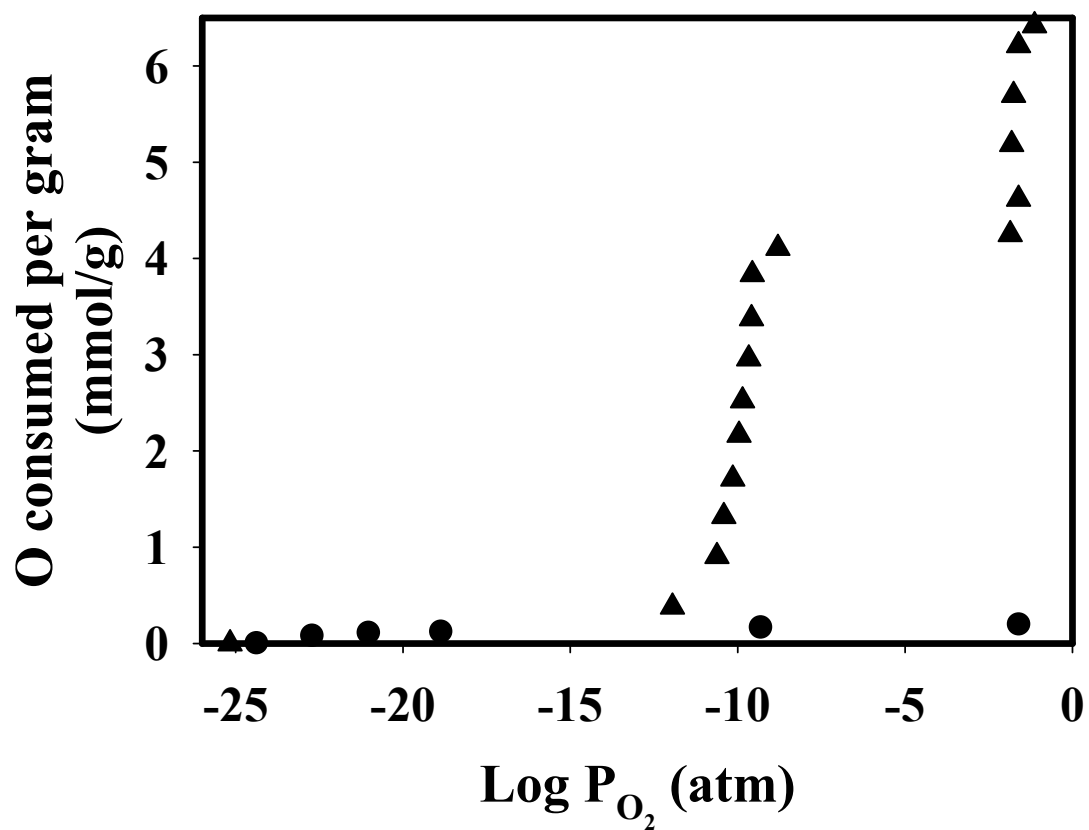


Figure 4. Oxygen consumed per gram of oxidized sample (mmol/g) as a function of $P(O_2)$ after the samples were reduced in 10% H_2 (balance N_2) at 973 K for 1 h. Results are shown for (●) CeO_2 and (▲) Mn_2O_3 .

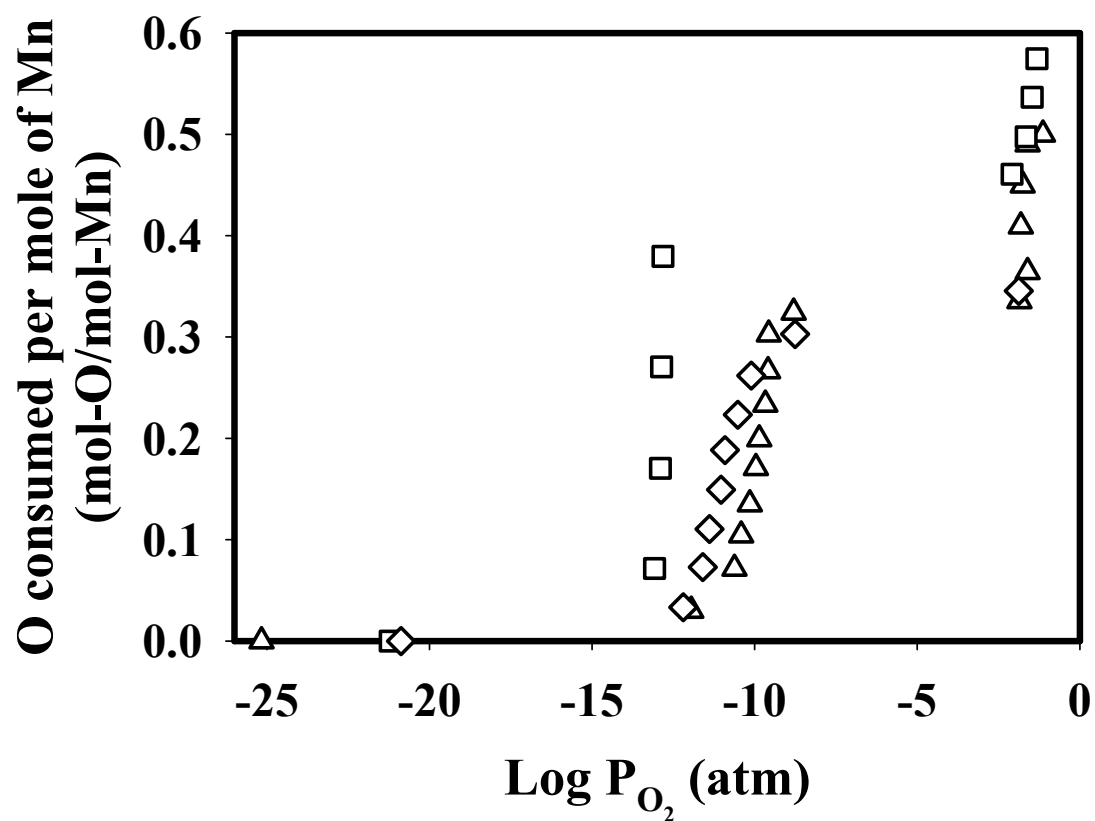


Figure 5. Oxygen consumed per mole of Mn (mol-O/mol-Mn) as a function of $P(O_2)$ after the samples were reduced in 10% H_2 (balance N_2) at 973 K for 1 h. Results are shown for (□) $Ce_{0.8}Mn_{0.2}O_{1.9}$, (◇) $Ce_{0.5}Mn_{0.5}O_{1.75}$, and (△) Mn_2O_3 .

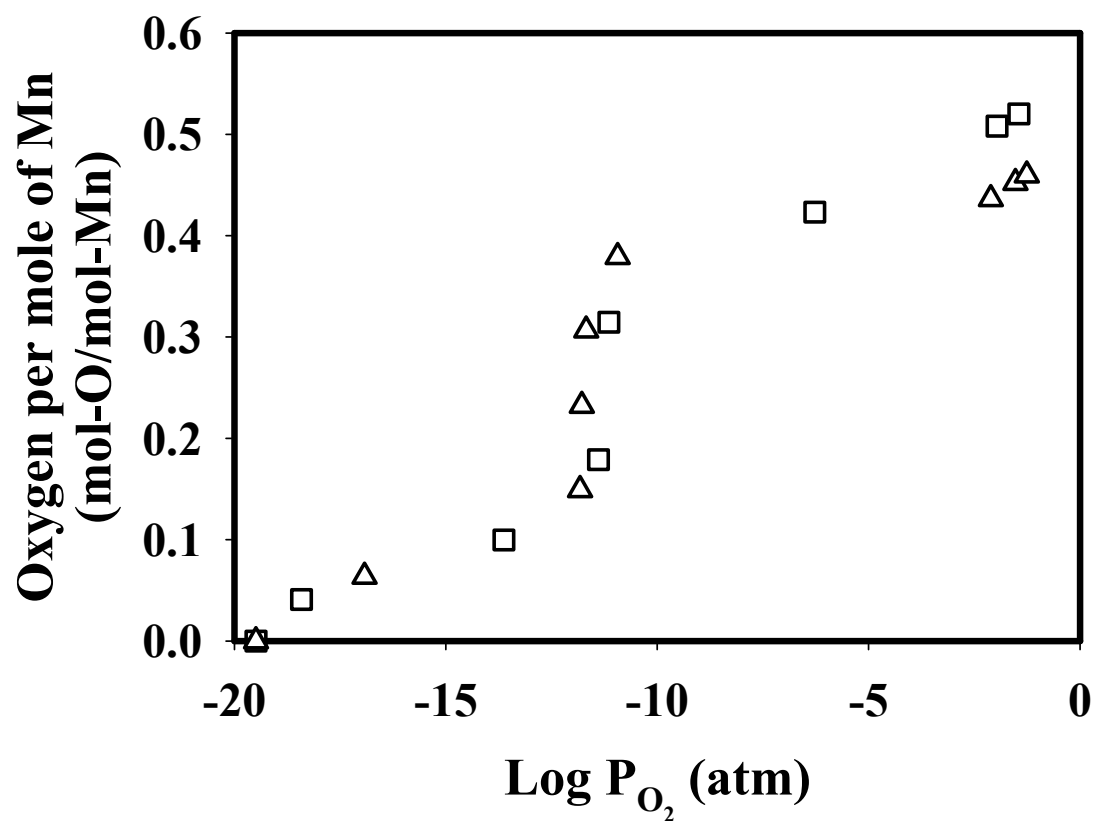


Figure 6. Oxygen per mole of Mn (mol-O/mol-Mn) for $\text{Ce}_{0.8}\text{Mn}_{0.2}\text{O}_{1.9}$ as a function of $P(\text{O}_2)$ at 973 K. The squares (□) were points measured by removing oxygen, starting from the fresh sample oxidized in 10% H_2O , 5% O_2 , and 85% Ar. The triangles (Δ) were measured by adding oxygen to the same sample.